nature communications

Article

https://doi.org/10.1038/s41467-024-51908-3

Reactive capture of CO_2 via amino acid

Received: 5 April 2024

Accepted: 19 August 2024

Published online: 08 September 2024

Check for updates

Yurou Celine Xiao[1,5], Siyu Sonia Sun[1,5], Yong Zhao[1], Rui Kai Miao[1], Mengyang Fan[1], Geonhui Lee[2], Yuanjun Chen[2], Christine M. Gabardo[1], Yan Yu[2], Chenyue Qiu[3], Zunmin Guo[1], Xinyue Wang[2], Panagiotis Papangelakis[1], Jianan Erick Huang[2], Feng Li[1], Colin P. O'Brien[1], Jiheon Kim[1,2], Kai Han[4], Paul J. Corbett[4], Jane Y. Howe[3], Edward H. Sargent[2] & David Sinton[1]

Reactive capture of carbon dioxide (CO_2) offers an electrified pathway to produce renewable carbon monoxide (CO), which can then be upgraded into long-chain hydrocarbons and fuels. Previous reactive capture systems relied on hydroxide- or amine-based capture solutions. However, selectivity for CO remains low (<50%) for hydroxide-based systems and conventional amines are prone to oxygen (O_2) degradation. Here, we develop a reactive capture strategy using potassium glycinate (K-GLY), an amino acid salt (AAS) capture solution applicable to O_2-rich CO_2-lean conditions. By employing a single-atom catalyst, engineering the capture solution, and elevating the operating temperature and pressure, we increase the availability of dissolved in-situ CO_2 and achieve CO production with 64% Faradaic efficiency (FE) at 50 mA cm^{-2}. We report a measured CO energy efficiency (EE) of 31% and an energy intensity of 40 GJ t_{CO}^{-1}, exceeding the best hydroxide- and amine-based reactive capture reports. The feasibility of the full reactive capture process is demonstrated with both simulated flue gas and direct air input.

The electrolysis of CO_2 presents a means to produce chemicals and industrial feedstocks, such as CO[1], while reducing atmospheric CO_2 levels by utilizing captured CO_2 from point sources or the air via direct air capture (DAC)[2,3]. Integrated CO_2 capture and conversion, a process known as reactive capture of CO_2, employs chemisorbed CO_2 in a post-capture solution as the feedstock – and thereby avoids CO_2 purification steps[4,5] and presents an opportunity for capital and energy cost savings[6]. Alkali hydroxide capture solutions provide high CO_2 absorption capacity, and are applicable to dilute-CO_2 and O_2-rich sources[7–9]. The strongly alkaline aqueous solution reacts with CO_2 to form carbonate ions (CO_3^{2-})[10,11]. Inside a reactive capture electrolyzer, CO_2 is regenerated from CO_3^{2-} via a pH swing using protons that electromigrated from the anode side. The regenerated CO_2 is subsequently electrochemically reduced into CO on the cathode. However, employing CO_3^{2-} feedstocks resulted in lower selectivities towards CO production (<50%) compared to other CO_2 electrolysis systems, despite strategies to modulate the cathode local pH and CO_2 concentration[12,13]. CO_2 is fundamentally limited in supply because the protons available for CO_2 regeneration are proportional to the applied current. CO_3^{2-} ions require 2 moles of protons to regenerate 1 mole of in-situ CO_2[14]. The reaction between in-situ CO_2 and local hydroxides (OH^-), a by-product of the CO_2 reduction reaction, reduces the concentration of in-situ CO_2 at the cathode[15].

To attain higher CO FE, more CO_2 is needed at the cathode. This can be achieved by using capture solutions that require less protons to regenerate in-situ CO_2. Amine solutions capture CO_2 in the forms of carbamate and bicarbonate, both of which require only 1 mole of protons to regenerate 1 mole of in-situ CO_2, which increases the CO_2 concentration and has resulted in CO FEs > 50%[16–18]. However, conventional amines used in carbon capture, such as monoethanolamine (MEA), are volatile and prone to O_2 degradation, rendering them unsuitable for capture in CO_2-dilute, O_2-rich environments such as air[19,20]. Bicarbonate formation via hydroxide-based capture has slow kinetics, which necessitates larger contactor areas and residence

[1]Department of Mechanical and Industrial Engineering, University of Toronto, Toronto, ON, Canada. [2]Department of Electrical and Computer Engineering, University of Toronto, Toronto, ON, Canada. [3]Department of Materials Science & Engineering, University of Toronto, Toronto, ON, Canada. [4]Shell Global Solutions International B.V., Amsterdam, The Netherlands. [5]These authors contributed equally: Yurou Celine Xiao, Siyu Sonia Sun.
e-mail: dave.sinton@utoronto.ca

times, leading to unfavorable process economics[21,22]. We sought a capture solution with a high CO_2 absorption rate (characteristic of amines), while also exhibiting low vapor pressure and O_2 tolerance (characteristic of hydroxides). We turned to AAS, a class of capture solutions with potential in this regard[23,24]. Typically prepared using equimolar amino acid and alkali hydroxide to form deprotonated amino acid anions with CO_2 capture capacity, their ionic nature makes them less volatile than MEA[25]. With these advantages, AAS-based CO_2 capture has been demonstrated, at the pilot plant scale, with excellent capture rate and stability[26,27]. Since the amino functional groups can capture CO_2 to form carbamate and bicarbonate, we thought them promising candidates for reactive CO_2 capture[28].

Here, we explored the reactive capture of CO_2 based on an AAS solution, potassium glycinate (K-GLY). Amongst amino acid candidates, K-GLY has shown particular promise for CO_2 capture with a unique combination of fast CO_2 capture kinetics and high CO_2 loading capacity at low CO_2 partial pressures (Supplementary Table 2)[28,29]. K-GLY is also low-cost, can be produced at scale, and presents a relatively low environmental impact[30]. The post-capture electrolyte is used directly as input to a membrane electrode assembly where CO is produced via the electrochemical reduction of in-situ generated CO_2. The K-GLY solution exhibits high O_2 tolerance and low evaporative loss compared to conventional amines. By engineering the catalyst, tuning the solution, and operating at an elevated temperature and pressure, we achieve a CO FE of 64% at an applied current density of 50 mA cm^{-2} and a measured full cell voltage of 2.74 V, corresponding to an EE of 31% towards CO. We demonstrate proof-of-concept by performing reactive CO_2 capture at ambient conditions with an applied current density of 50 mA cm^{-2} using atmospheric air containing ~400 ppm of CO_2 and 21% O_2, and using a simulated flue gas stream containing 15% CO_2 and 15% O_2, achieving a maximum CO FE of 19% and 51%, respectively.

Results and discussion

O_2 degradation and evaporative loss of amine-based capture solutions

Carbon capture solutions are exposed to high concentrations of O_2, ranging from 1 to 15% in flue gas and 21% in ambient air[31]. For DAC, the capture solutions are also subject to high air flows due to the comparatively low concentration of CO_2 in the atmosphere[7]. We compared the static O_2 tolerance of three amine-based capture solutions: MEA, 2-amino-2-methyl-1-propanol (AMP) – a sterically hindered primary alkanolamine with improved O_2 tolerance[32], and K-GLY. We exposed each capture solution to 100 sccm of air at an elevated temperature of 55 °C and with 600 rpm of stirring to expedite the degradation process while maintaining a regime where O_2 and thermal degradations can be decoupled (Supplementary Figs. 1 and 2)[20]. The amount of amine lost after 7 days was measured and the degree of O_2 degradation was quantified by measuring the concentrations of known degradation products: ammonia, formate, oxalate, nitrate, and nitrite (Table 1)[33–35].

We found that MEA experienced the most severe O_2 degradation, evidenced by the large quantity of produced ammonia, a marker for amine degradation (Supplementary Fig. 3)[20]. The extent of MEA O_2 degradation can also be corroborated by its linearly increasing formate concentration compared to the relatively steady formate concentrations of AMP and K-GLY (Supplementary Figs. 4–6). ^{1}H NMR analysis of the capture solutions before and after 7 days was used to quantify the amount of amine lost due to the combination of O_2 degradation and evaporation (Supplementary Fig. 7). MEA and AMP lost 29.2 mmol mol^{-1} and 31.6 mmol mol^{-1} of amine, respectively. AMP had the greatest amine loss, a result we attribute to its high volatility[36]. In contrast, K-GLY lost 16.7 mmol mol^{-1} of amine, a little over half the loss incurred with the alkanolamines. K-GLY exhibited the highest O_2 tolerance and amine retention, making it a suitable capture solution for carbon capture processes with high levels of O_2 and low CO_2 concentrations.

Table 1 | Amine loss and degradation product concentrations for the O_2 degradation of MEA, AMP, and K-GLY

Amine	Amine loss (mmol mol^{-1})	Ammonia	Formate	Oxalate	Nitrate	Nitrite
Expedited static degradation (55 °C, 600 rpm, 100 sccm of air)						
3 M MEA	29.2	0.15	1.29	0.02	0.25	1.41
3 M AMP	31.6	0.012	0.15	0.05	–	1.87
3 M K-GLY	16.7	0.002	0.14	–	–	1.53
Degradation under electrolysis (ambient, no stirring, 100 sccm of air, 50 mA cm^{-2})						
2 M K-GLY + 0.1 M KH_2PO_4	7.7	0.0006	0.31	–	–	–

Integrated CO_2 capture and conversion

In the integrated system, CO_2-rich post-capture solution is fed into an electrolyzer where CO electro-production and capture solution regeneration occur simultaneously, and CO_2-lean capture solution is subsequently returned to the carbon capture unit (Fig. 1). The reactions involved in the capture and conversion processes are represented by Supplementary Eqs. (1)–(9) in Supplementary Fig. 8. In the carbon capture unit, an anionic glycinate reacts with CO_2 to form a glycine-carbamic acid, which is then deprotonated by a second glycinate to form a glycine-carbamate and a glycine zwitterion (Supplementary Eq. (1))[30]. The hydrolysis of glycine-carbamate, at a sufficiently high CO_2 loading, forms an equilibrium of glycine-carbamate, bicarbonate, and glycinate (Supplementary Eq. (2) and Supplementary Fig. 9)[29]. The post-capture solution used for electrolysis has a pH of 8.1 and consists of 60% bicarbonate (Supplementary Fig. 10). Inside the electrolyzer, CO_2 is released from the chemisorbed forms, glycine-carbamate or bicarbonate, via pH swing with the addition of protons that electromigrated across the cation exchange membrane (CEM) from the anode side (Supplementary Eqs. (3) and (4)). The glycinate regenerated in Supplementary Eqs. (2) and (3) can capture additional CO_2. A CO_2 diffusion layer between the CEM and the cathode catalyst is added to maintain an alkaline local environment at the cathode for efficient CO_2 conversion[37]. The in-situ CO_2 reacts on the cathode catalyst to produce CO and OH^- (Supplementary Eq. (5)). In an alkaline environment (>pH 9.6)[38], OH^- deprotonates the glycine zwitterion from Supplementary Eq. (1) to form glycinate (Supplementary Eq. (6)) and regenerate the K-GLY solution. The in-situ CO_2 can also react with the produced OH^- to form (bi)carbonates via Supplementary Eqs. (7) and (8), limiting the cathode's local CO_2 concentration[15]. On the anode side of the electrolyzer, acidic oxygen evolution reaction (OER) takes place and produces the protons required for in-situ CO_2 formation (Supplementary Eq. (9)).

Silver (Ag) is a highly selective electrocatalyst used in gas-phase CO_2 electrolysis and hydroxide-based reactive capture of CO_2 to produce CO. However, when used in reactive capture with 1 M K-GLY as the capture solution, its selectivity towards CO was low. The Ag catalyst has a relatively negative potential of zero charge (PZC) which may have resulted in a reduced cathode surface charge density in the presence of bulky glycine ions, leading to unstable CO_2 reduction intermediates. A single-atom catalyst with more positively shifted PZC could increase the surface cation charge density and improve conversion efficiency[17]. Compared to transition metal catalysts such as Ag and gold, carbon-supported single-atom catalysts also have higher catalytic activities through stabilization of larger dipole moments on reaction intermediates[39]. We synthesized a zeolitic imidazolate framework (ZIF)–8-derived nickel single-atom (Ni-N/C) catalyst for amine-based reactive capture which significantly improved the CO FE (Supplementary Fig. 11). The catalyst composition was optimized by tuning the nickel weight percent during catalyst synthesis, the Ni-N/C loading onto the current conducting substrate, and the ionomer content in the catalyst solution mixture (Supplementary Fig. 12). The Ni-N/C catalyst

https://doi.org/10.1038/s41467-024-51908-3

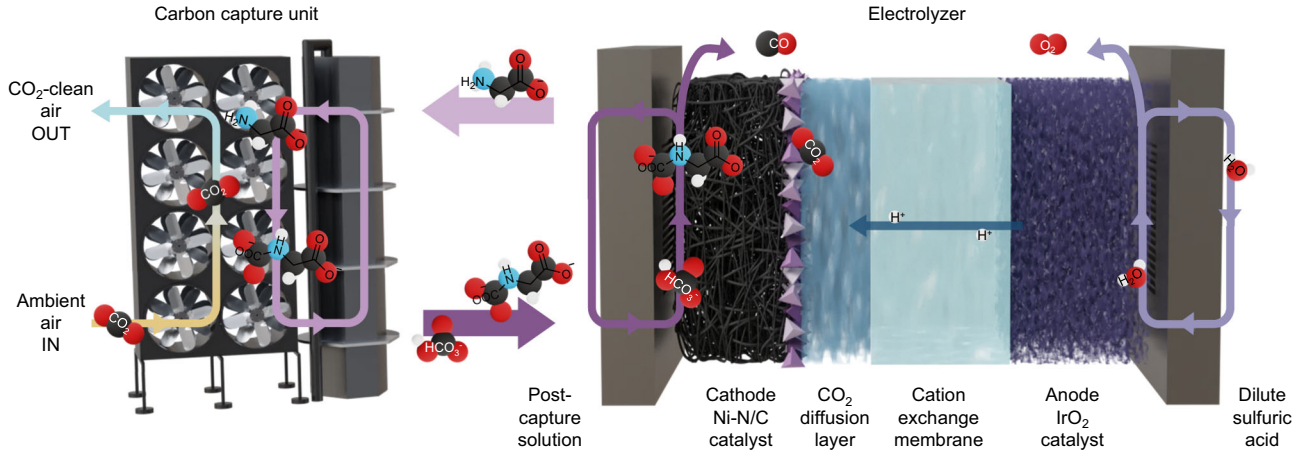

Fig. 1 | Schematic of the reactive capture system using K-GLY as the capture solution. The left panel depicts a carbon capture unit used to capture CO_2 from the atmosphere via DAC. The right panel depicts a membrane electrode assembly used for CO_2 electrolysis. The capture solution is circulated between the two units.

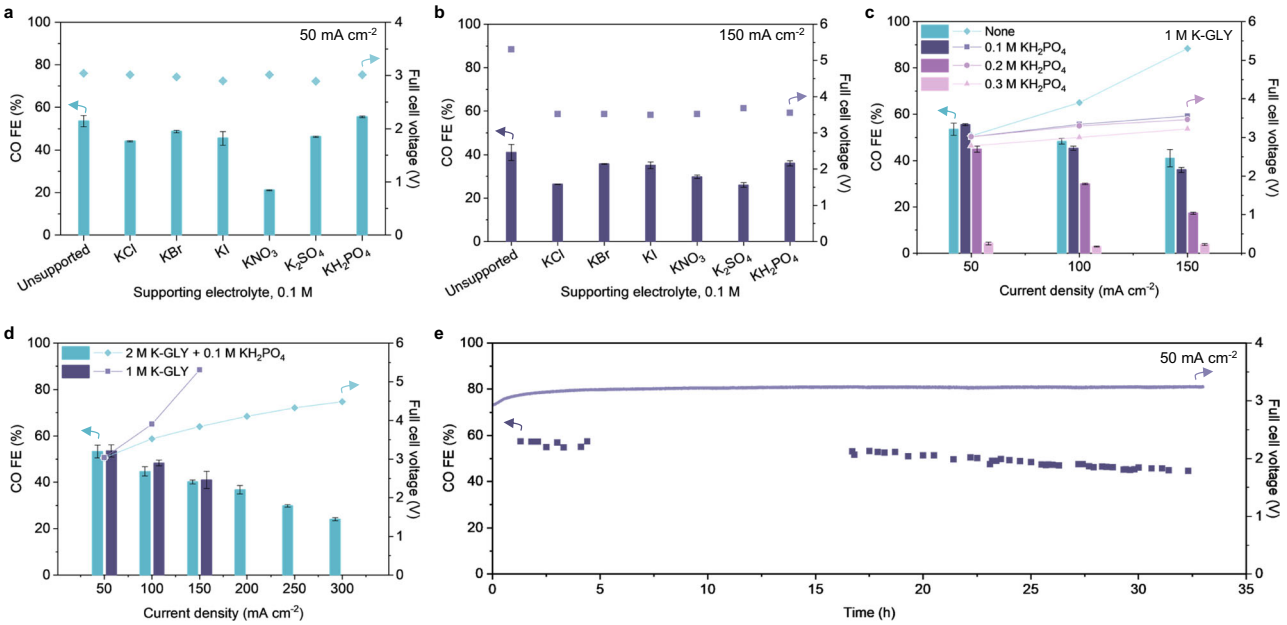

Fig. 2 | Optimization of the capture solution and system stability. a, **b** FE towards CO and full cell voltage for a 1 M K-GLY capture solution with 0.1 M of various supporting electrolytes: potassium chloride (KCl), potassium bromide (KBr), potassium iodide (KI), potassium nitrate (KNO_3), potassium sulfate (K_2SO_4), and monopotassium phosphate (KH_2PO_4). **c** FE towards CO and full cell voltage for a 1 M K-GLY capture solution with KH_2PO_4 supporting electrolyte concentration varying from 0 to 0.3 M. **d** FE towards CO and full cell voltage for an unsupported 1 M K-GLY capture solution and the optimized capture solution (2 M K-GLY with 0.1 M KH_2PO_4). **e** stability test of reactive CO_2 capture for 32 h at an applied current density of 50 mA cm^{-2} using 1 L of catholyte and anolyte. Error bars represent the standard deviation of at least three independent measurements. Source data are provided as a Source Data file.

also exhibited excellent selectivity towards CO when a pure bicarbonate solution was used as the catholyte (Supplementary Fig. 13), demonstrating its high catalytic activity across various carbon-containing electrolytes. The nickel dispersion was characterized using x-ray diffraction analysis (XRD) (Supplementary Fig. 14) and scanning transmission electron microscopy (STEM) (Supplementary Fig. 15). The increase in CO selectivity when employing the Ni-N/C catalyst demonstrated the need for CO_2 reduction catalysts specific to amine-based reactive capture; highly selective gas-phase CO_2 catalysts are not directly applicable to the amine-based integrated system.

Capture solution design

Glycine-carbamate is a bulky compound compared to other chemisorbed forms of CO_2 such as (bi)carbonate (Supplementary Table 3). The electrical property of capture solutions – while not a consideration in conventional CO_2 capture – is important in reactive capture where the capture solution also serves as an electrolyte. We explored potassium salt additives to increase the ionic conductivity of the K-GLY capture solution. Potassium was chosen as the supporting electrolyte cation to match the cation of the AAS. We operated the electrolyzer under constant applied current and found that the supporting electrolyte did not have a significant effect on full cell voltage at 50 mA cm^{-2} (Fig. 2a). However, at a higher current density of 150 mA cm^{-2}, the full cell voltage with the modified electrolyte was more than 1.5 V lower than that of the unmodified case, for all potassium salts tested (Fig. 2b). With the exception of potassium nitrate (KNO_3), the addition of supporting potassium salts maintained ~100% combined FE of CO and hydrogen (H_2) (Supplementary Fig. 16). When KNO_3 was employed as the supporting electrolyte, the selectivity towards CO and H_2 both decreased due to the thermodynamically

more favorable nitrate reduction reaction[40–42]. We selected monopotassium phosphate (KH_2PO_4) as the supporting electrolyte because it maintained a relatively high CO selectivity across a wide range of current densities from 50 to 300 mA cm^{-2} (Supplementary Fig. 17). The buffering capacity of 0.1 M KH_2PO_4 may also aid in stabilizing the pH in the CO_2 diffusion layer and thereby increase CO FE[13]. In the absence of the CO_2 capture agent, anionic glycinate, we observed only H_2 and no CO production (Supplementary Fig. 18). This observation indicated that glycine in the zwitterion form has no CO_2 capture abilities and is not the reactive carbon source. K_2HPO_4 also does not capture CO_2 and primarily functions to improve electrolyte conductivity.

We then assessed the effect of supporting electrolyte concentration and found that increasing the KH_2PO_4 molarity beyond 0.1 M yielded small reductions in the full cell voltage, albeit at a severe cost to CO selectivity (Fig. 2c). One reason for this phenomenon could be that phosphate has a high buffering capacity which, at higher concentrations, suppresses the acidic environment needed for in-situ CO_2 generation and simultaneously acts as a proton donor for HER[43,44]. We probed the electrolyzer using electrochemical impedance spectroscopy (EIS) and found that the addition of 0.1 M KH_2PO_4 reduced both the series and charge transfer resistances, and that higher KH_2PO_4 concentrations did not significantly change the shape of the low-frequency semicircle (Supplementary Fig. 19). Employing a 0.1 M KH_2PO_4 supporting electrolyte, we examined the concentration effect of the capture solution and found that the 2 M K-GLY capture solution achieved the highest CO FE at current densities above 150 mA cm^{-2} (Supplementary Fig. 20). The 3 M K-GLY capture solution did not provide the highest CO FE despite having the highest amount of chemisorbed CO_2 (Supplementary Table 4). We reasoned that the glycine zwitterion, which exists in equal molarity to the glycine-carbamate in Supplementary Eq. (1), contains an ammonium cation group that can enhance HER[45,46]. Thus, the design of the capture solution for high CO selectivity should consider the solution equilibria and the concentrations of all proton-donating species, including the supporting electrolyte and by-products formed during CO_2 capture[47,48].

The optimized capture solution, consisting of 2 M K-GLY and 0.1 M KH_2PO_4, maintained similar CO selectivity compared to the 1 M K-GLY unsupported capture solution while providing a low full cell voltage (Fig. 2d). A lower cell voltage results in higher EE towards CO and enables high current density operations. We varied the catholyte and anolyte flow rates and found that increasing the catholyte flow rate increased the CO selectivity via improved mass transfer which balanced the cathode local pH and CO_2 availability (Supplementary Fig. 21)[13]. To evaluate the stability of the electrolyzer, we first demonstrated a batch process where the catholyte and anolyte were refreshed in 5- to 7-h intervals (Supplementary Fig. 22). The CO FE improved after refreshing the electrolytes. Liquid analysis of the catholyte after 5 h of electrolysis revealed that the CO_2 loading decreased from 0.67 to 0.49 mol_{CO2} $mol_{K\text{-}GLY}^{-1}$, with the bicarbonate concentration decreasing from 60% to 35% of the overall chemisorbed CO_2 species (Supplementary Fig. 23). These results indicated that the initial decline in CO FE was due to the reduced concentration of bicarbonate as it shifts towards CO_2 in the diffusion layer and converts into CO. We then demonstrated the stability of the system with increased catholyte and anolyte volumes and maintained a CO FE > 45% over 32 h of electrolysis at a constant applied current density of 50 mA cm^{-2} (Fig. 2e and Supplementary Fig. 24). This level of stability is competitive with the state-of-the-art in amine-based reactive capture. However, extending stability for CO_2 conversion systems, especially those directly employing capture solutions, remains a challenge for the field.

Temperature and pressure effects

In previous amine-based reactive capture systems, increasing the reaction temperature increased the CO FE[17,49]. CO_2 desorption from amine-based capture solutions is an endothermic process[50]. Therefore, adding thermal energy to the system can accelerate the rate of in-situ CO_2 generation. The addition of heat can also lower the viscosity of the electrolyte, improving overall mass transfer within the system[51]. However, at higher temperatures, the solubility of CO_2 in aqueous solutions decreases according to Henry's law[52]. This results in CO_2 bubble formation when the saturated solubility is exceeded, and a lower concentration of dissolved CO_2 is available for conversion. We tested the hypothesis that dissolved in-situ CO_2 was the active species by replacing the acidic anolyte with 1 M potassium hydroxide (KOH) that would suppress CO_2 regeneration. We found no quantifiable amount of CO at 20 °C (Supplementary Fig. 25), suggesting that the chemisorbed CO_2 in the forms of glycine-carbamate and bicarbonate do not participate in the reduction reaction to form CO, in agreement with recent works[17,45,46,53]. When we increased the operating temperature to 40 and 60 °C, we saw a slight shift in selectivity towards CO (<3%) which we attributed to small amounts of CO_2 regenerating via temperature-swing. The concentration of the reactant, dissolved in-situ CO_2, could be increased by improving the CO_2 solubility via increased system pressure, an approach that was beneficial in an integrated system using bicarbonate as the electrolyte[40]. We posited that simultaneously elevating the temperature and pressure of the system would improve the CO EE by increasing the CO_2 availability at the cathode and decreasing the overall electrolyzer resistance.

We operated the electrolyzer between temperatures of 20–45 °C and pressures of 1 to 5 bar under a constant applied current density of 50 mA cm^{-2} (Fig. 3a, b). We found that at atmospheric pressure, increasing the temperature decreased the CO FE. Though temperature increased the rate of CO_2 regeneration, it also decreased CO_2 solubility, which led to less net dissolved CO_2 available for conversion (Supplementary Table 5). At elevated pressures of 3 to 5 bar, an increase in temperature from 20 to 35 °C improved the CO selectivity. We reached an optimal operating condition at 4 bar and 40 °C, yielding a maximum CO FE of 64%, and measured full cell voltage of 2.74 V, a 11% and 0.3 V improvement compared to the CO FE and voltage at ambient conditions (1 bar and 20 °C), respectively. Further increases in temperature substantially increased hydrogen evolution reaction (HER) kinetics and significantly decreased CO selectivity[54]. At the optimal operating condition of 4 bar and 40 °C, the CO FE was higher, and the full cell voltage was lower than those at ambient conditions for all current densities between 50 to 200 mA cm^{-2} (Fig. 3c). In previous reactive capture systems, the reaction potential versus a reversible hydrogen electrode (RHE) was reported when the catalytic performance was evaluated in an H-cell or flow cell[16,17,49,51]. These electrolyzer architectures have high electrolyte resistance, are limited in current density, and the resulting overall EE, when calculated, is low[55]. We operated reactive capture in a membrane electrode assembly to overcome these challenges and enable energy-efficient CO production. The simultaneous elevation of temperature and pressure, together with the engineered catalyst and electrolyte, enabled a maximum CO EE of 31% at an applied current density of 50 mA cm^{-2} – performance that exceeds hydroxide – and amine-based reactive capture efforts to date (Fig. 3d, Supplementary Table 6, and Supplementary Fig. 26). We achieved a maximum CO partial current density (j_{CO}) of 89 mA cm^{-2} at an applied commercially-relevant current density of 200 mA cm^{-2} (Fig. 3d)[56], surpassing best prior amine-based reports.

Energy cost analysis

To evaluate the potential of amine-based reactive CO_2 capture towards CO using a K-GLY capture solution, we compared the energy expenditure of this work to alternative CO_2 electrolysis systems (Table 2, Supplementary Note 1, and Supplementary Table 1). The processes considered include CO_2 capture for the initial feedstock, CO_2 electrolysis to produce CO, and CO_2 recovery to separate excess CO_2 from CO and H_2 in the cathode product gas stream. The energy required to generate 1 tonne of CO was 40 GJ for K-GLY-based reactive capture,

https://doi.org/10.1038/s41467-024-51908-3

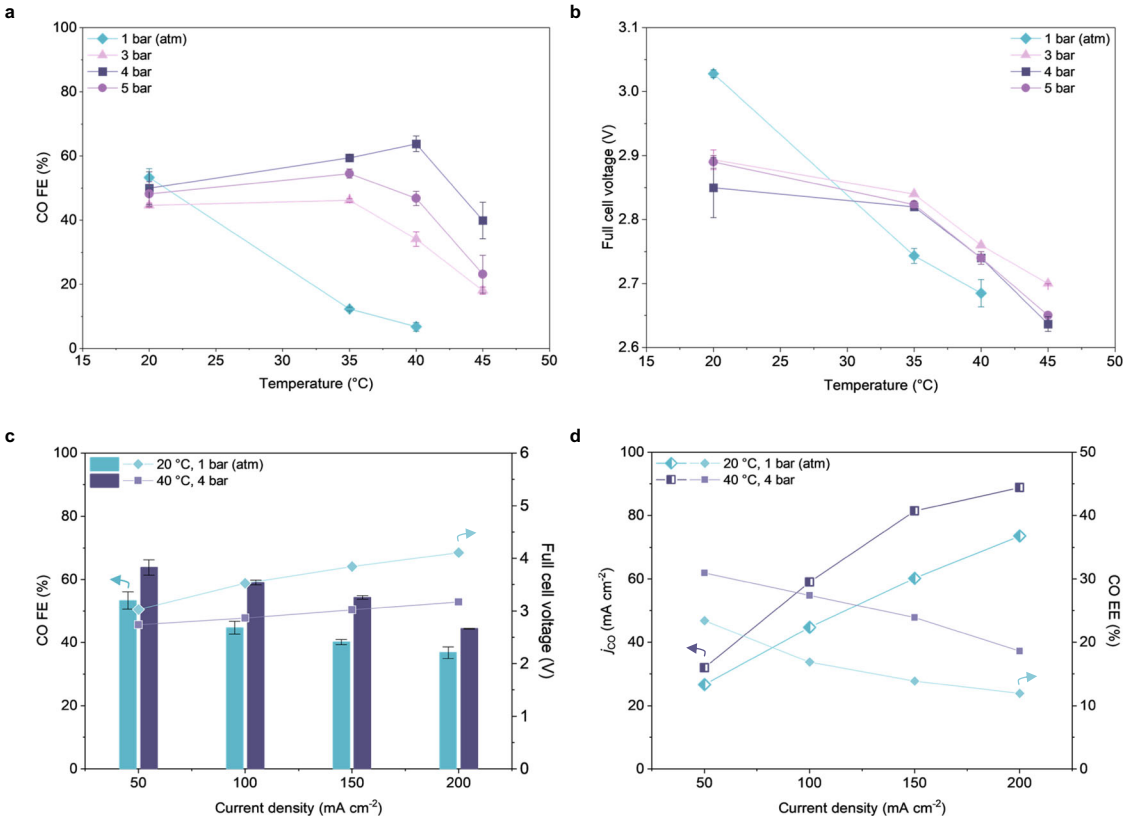

Fig. 3 | Effects of increased temperature and pressure. a FE towards CO and **b**, full cell voltage at an applied current density of 50 mA cm^{-2} for a 2 M K-GLY with 0.1 M KH_2PO_4 capture solution at pressures between 1 to 5 bar and temperatures between 20 to 45 °C. **c** FE towards CO and full cell voltage and **d**, j_{CO} and EE towards CO for a 2 M K-GLY with 0.1 M KH_2PO_4 capture solution at atmospheric conditions (20 °C and 1 bar) and at the optimal elevated conditions (40 °C and 4 bar). Temperature was measured at the outlet of the cathode, and pressure was measured at the gaseous downstream of the cathode. Error bars represent the standard deviation of at least three independent measurements. Source data are provided as a Source Data file.

Table 2 | Comparison of energy towards CO for gas-phase CO_2 electrolysis, hydroxide- and amine-based reactive capture

System	Gas-phase CO_2 electrolysis	Hydroxide-based reactive capture	Amine-based reactive capture (this work)
CO_2 capture (GJ t_{CO}^{-1})	10.3	0.5	0.5
Electrolysis (GJ t_{CO}^{-1})	23.0	56.3	29.7
CO_2 utilization (%)	25	100	9
CO_2 recovery (GJ t_{CO}^{-1})	21.7	0	10.0
Total (GJ t_{CO}^{-1})	55.0	56.8	40.2

which was 27% less than gas-phase CO_2 electrolysis[1,57,58] and 29% less than hydroxide-based reactive capture[13]. The largest energy expenditure for this work was electrolysis energy (30 GJ t_{CO}^{-1}) at 74% of the total – motivating additional efforts to reduce cell voltage and improve CO selectivity. The CO_2 recovery energy was calculated using the measured CO_2 utilization and accounted for 25% of the total energy (10 GJ t_{CO}^{-1}). Unconverted gas-phase CO_2 in the product stream must be recovered to purify the gas products and recycle the CO_2 reactant[5]. The CO_2 utilization represents the ratio between converted and total CO_2 measured in the cathode gas stream. The CO_2 utilization increased from 8.6% to 45.5% by increasing the current density from 50 to 200 mA cm^{-2} to increase overall CO_2 conversion rates and lowering the temperature from 40 to 20 °C to reduce excess CO_2 in the cathode (Supplementary Fig. 27). Improving the CO_2 utilization lowered the CO_2 recovery energy from 10 to 1 GJ t_{CO}^{-1}. Therefore, in addition to CO EE, achieving a high CO_2 utilization is essential to lowering the overall operational energy of the reactive capture system. Operational energy costs are important to consider as they typically account for the majority of the total cost in CO_2 electrolysis technologies[59]. A comprehensive evaluation of the total costs (capital and operational expenditures) requires a significant increase in scale, current density, and stability. The reactive capture system has the potential to improve in these metrics as it shares many similarities in electrolyzer architecture with matured and scaled-up water and gas-phase CO_2 electrolysis technologies[60–62]. The stability and scalability of amino acid-based CO_2 capture were previously demonstrated at the pilot scale[26,27].

CO_2 sourced from the atmosphere and simulated flue gas

To demonstrate the industrial applicability of the AAS reactive capture system, we tested it with dilute CO_2 feeds. We adapted a humidifier to capture air from our laboratory for DAC experiments (Supplementary Fig. 28)[63]. To simulate point source capture, we employed a mixed gas stream comprising of 15% CO_2 and 15% O_2 balanced with nitrogen (N_2) (Supplementary Table 7)[31]. Using the optimized capture solution (2 M K-GLY and 0.1 M KH_2PO_4) in both experiments, we recorded the pH of the capture solution as it captured CO_2 from dilute feeds, until a plateau in pH was reached (Fig. 4a). The pH values of the DAC and

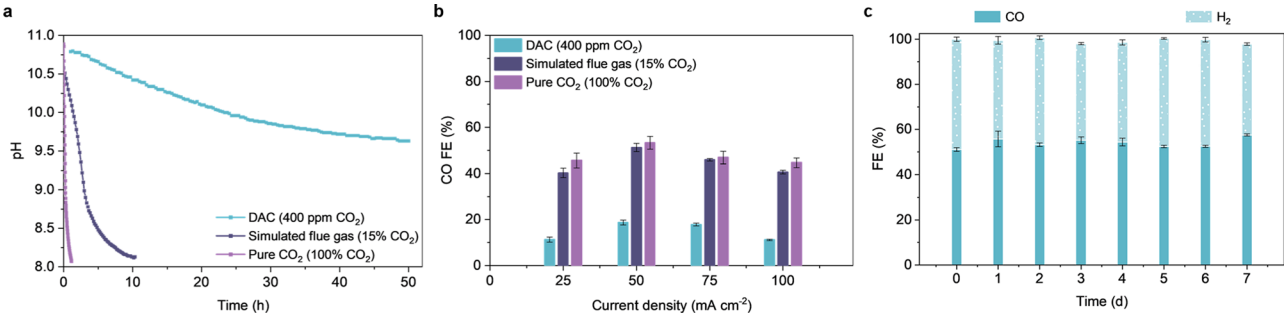

Fig. 4 | Demonstration of the AAS-based reactive capture with low-CO_2 high-O_2 conditions. a pH of a 2 M K-GLY with 0.1 M KH_2PO_4 capture solution over time while capturing CO_2 from the atmosphere (400 ppm), CO_2 from a simulated flue gas (15%), and pure CO_2 (100%). **b** FE towards CO using the post-capture solutions of the capture processes in **a**. **c** FE towards CO and H_2 of a newly assembled electrolyzer while continuously operating at 50 mA cm^{-2} and exposing the same capture solution to 100 sccm of air for 7 days. The applied current was paused daily for a maximum of 5 min while the electrolyzer assembly was replaced with a new one. The electrolyzer was operated at ambient conditions (1 bar and 20 °C). Error bars represent the standard deviation of at least three independent measurements. Source data are provided as a Source Data file.

simulated flue gas experiments plateaued at 9.6 and 8.1, respectively. The difference in the equilibrium pH values was due to different CO_2 partial pressures[45]. We then fed the post-capture solutions into the electrolyzer to achieve a maximum CO FE of 19% for the DAC experiment and a maximum CO FE of 51% for the simulated flue gas experiment (Fig. 4b). The limited concentration of CO_2 in the atmosphere, which resulted in a lower amount of chemisorbed CO_2 in the DAC post-capture solution, yielded in a lower CO FE. The CO selectivities for the simulated flue gas feed and pure CO_2 feed were comparable, demonstrating feasibility of reactive capture with dilute CO_2 inputs when using AAS as the capture solution. We also investigated the O_2 tolerance of the capture solution under continuously reducing conditions by circulating the capture solution through an electrolyzer operated at 50 mA cm^{-2} while exposing the solution to 100 sccm of air for 7 days (Supplementary Fig. 29). A new electrolyzer was assembled daily to decouple the degradation of the electrolyzer and the capture solution. The selectivity towards CO each day remained consistent ~50% and no FE towards the O_2 reduction reaction (ORR) was observed due to the hydrophilic nature of the reactive capture system and low O_2 solubility (Fig. 4c)[64]. Compared to the expedited static degradation of K-GLY, degradation under electrolysis was less severe, evidenced by the reduced amine loss and degradation product concentrations (Table 1 and Supplementary Fig. 30).

In summary, we pursued energy-efficient electro-production of CO in a reactive capture system applicable to high-O_2 low-CO_2 conditions typical of point sources and air. Previous hydroxide-based reactive capture exhibited low selectivity towards CO (<50%) due to a limit on in-situ CO_2 generation. Amine-based reactive capture provides higher CO FE but the conventional capture solution, MEA, degrades in O_2-rich environments. We compared different amine-based capture solutions and found that K-GLY exhibited the lowest solvent loss due to O_2 degradation and evaporation, making it a suitable capture solution for O_2-rich CO_2-lean sources. To achieve energy-efficient CO_2 conversion, we employed a nickel single-atom catalyst, optimized the capture solution, and engineered a reactive capture system at elevated temperatures and pressures to increase CO_2 availability at the cathode. As a result, we achieved CO production with CO FE of 64% and CO EE of 31% at 50 mA cm^{-2}, pressure of 4 bar, and temperature of 40 °C, surpassing the EE of hydroxide- and amine-based reactive capture reports to date. The combination of catalyst, electrolyte, and system engineering allowed us to sustain high CO selectivity at an industrially relevant current density of 200 mA cm^{-2}, obtaining a j_{CO} of 89 mA cm^{-2}. We compared the energy intensity towards CO of this work (40 GJ t_{CO}^{-1}) to gas-phase CO_2 electrolysis and hydroxide-based reactive capture and found energy savings of 27% and 29%, respectively. We assessed the feasibility of reactive capture using ambient air and simulated flue gas stream and achieved a maximum CO FE of 19% and 51%, respectively. This work offers a pathway to integrated CO_2 capture and conversion, from the largest CO_2 sources to major carbon-based product markets.

Methods

Materials

Unless otherwise specified, all reagents were purchased from commercial suppliers without further purification. Milli-Q water with a resistivity of 18.2 MΩ cm at 25 °C was used for all experiments.

O_2 degradation

The oxidative degradation of amines is often studied under forced oxidation conditions to accelerate the process[19]. For expedited static degradation experiments, 250 mL of 3 M capture solution (MEA, AMP, and K-GLY) was placed on a magnetic stirrer with temperature-probe-controlled heating at 55 °C and stirring speed set to 600 rpm. Instrument air, with approximately the same composition as atmospheric air (21% O_2 and 400 ppm CO_2), was purged into the capture solution at a constant flowrate of 100 sccm. For degradation under electrolysis experiments, 300 mL of the capture solution (2 M K-GLY and 0.1 M KH_2PO_4) was circulated through the cathode of a reactive capture electrolyzer operated at 50 mA cm^{-2} while instrument air was continuously purged through the capture solution at a constant flowrate of 100 sccm. Once a day, the capture solution was purged with pure CO_2 until a pH of 8.1 was reached. Then, the applied current was paused for a maximum of 5 minutes while the electrolyzer was replaced with a newly assembled one and the liquid samples were collected. The gas samples were collected daily after at least 20 minutes of operating the new electrolyzer for complete removal of dissolved CO_2 and even mixing of gaseous products. The anolyte was refreshed daily.

For all degradation experiments, the headspace of the capture solution was connected to a 40 mL deionized (DI) water trap to capture volatile chemicals including amines and degradation products. The headspace of the DI water trap was open to the atmosphere. Experiments were each performed over 7 days. Each day, a liquid sample was taken from the capture solution. Then, water from the DI water trap was poured into the capture solution to replace the removed and evaporated water until the capture solution refilled to its original volume. Fresh DI water was then added to the DI water trap until it refilled to 40 mL. The liquid from the DI water trap was collected at the end of the 7-day experiment. All liquid samples were stored in a refrigerator at 0 °C to minimize further degradation prior to analysis.

Ni-N/C catalyst preparation

3.39 g of zinc nitrate hexahydrate was dissolved in 180 ml of methanol. 3.94 g of 2-methylimidazole was dissolved in 180 ml of methanol in a separate container and added to the zinc nitrate hexahydrate solution. The mixture was continuously stirred at 500 rpm and 60 °C for 24 h. The ZIF-8 powder was collected by centrifuging the mixture, washing with methanol 3 times, and drying under a vacuum at 60 °C overnight. 100 mg of the prepared ZIF-8 power was then dispersed in 12 ml of n-hexanes and sonicated for 1 h at room temperature. After forming a homogeneous suspension, 330 µl of 0.1 M nickel (II) nitrate hexahydrate was added dropwise to the sonicating solution at room temperature. The nickel-doped solution was centrifuged, washed with methanol three times, and dried under a vacuumed at 60 °C overnight. The collected powder was placed in a tube furnace and heated to 900 °C for 2 h under constant argon (Ar) flow to yield the Ni-N/C catalyst.

Ni-N/C catalyst characterization

XRD was performed using a Rigaku Miniflex diffractometer with Cu Kα radiation (1.5405 Å) to identify the phase information and crystallinity of the catalyst. The XRD patterns were obtained with a step width of 0.2° 2θ and a speed of 5° per minute. All other parameters were chosen to enhance the signal-to-noise ratio in the data. STEM was performed using a Hitachi HF3300 equipped with a cold field emission electron gun and a Bruker silicon-drift energy dispersive X-ray spectroscopy (EDS) detector, operated at an accelerating voltage of 300 kV. The STEM images were acquired using secondary electron (SE), Z-contrast (ZC), and bright field (BF) modes simultaneously with a convergence angle of 18 mead in high-resolution mode. The samples were diluted with methanol and the suspension was drop-casted onto a holey carbon film supported on Cu grids.

Electrolyzer operation

The cathode electrode was fabricated by spray-coating a Ni-N/C catalyst ink onto hydrophilic carbon paper (AvCarb MGL190, Fuel Cell Store). The Ni-N/C ink for a 6.25 cm^2 substrate was prepared by dispersing 25 mg of Ni-N/C catalyst and 75 mg of Nafion dispersion (5 wt.%, Fuel Cell Store) in 2 ml of methanol and sonicating for 1 h before spray-coating. A catalyst loading of ~1 mg cm^{-2} was achieved. For the Ag catalyst, the Ag ink for a 6.25 cm^2 substrate was prepared by dispersing 50 mg of Ag nanoparticles (99.99%, 20 nm, US Research Nanomaterials) and 150 mg of Nafion dispersion in 2 ml of methanol and sonicating for 1 h before spray-coating. A catalyst loading of ~2.5 mg cm^{-2} was achieved. The prepared catalyst was used as the cathode electrode with an exposed area of 1 cm^2. Titanium-supported iridium oxide (Magneto Special Anodes, Evoqua Water Technologies) was used as the anode electrode. The cathode and anode electrodes were separated by a Nafion membrane (N117, Ion Power), with an additional layer of mixed cellulose ester (MCE) membrane filter (8.0 µm pore size, Millipore Sigma) or polytetrafluoroethylene (PTFE) membrane filter (5.0 µm pore size, Millipore Sigma) as the CO_2 diffusion layer added between the cathode electrode and the membrane. Nafion membranes were activated via the following procedure: 1 h at 90 °C 3 wt.% H_2O_2, 1 h in 90 °C DI water, 1 h in 90 °C 5 wt.% H_2SO_4, and 1 h in 90 °C DI water again. The activated Nafion membranes were stored in DI water.

All electrochemical experiments were conducted using a membrane electrode assembly with data collected using a potentiostat (Autolab PGSTAT204). Post-capture solution consisting of K-GLY with different molar concentrations, with and without supporting electrolyte, was circulated as the catholyte. In a typical experiment, 75 mL of the capture solution was purged with 80 sccm of 100% CO_2 until a pH of 8.1 has been reached. The pH of the solution was measured using a pH/conductivity meter with accuracy of ±0.01 (PC8500, Apera Instruments). The amount of CO_2 captured was quantified by weighing the capture solution before and after purging. The anolyte was 75 mL of 0.05 M sulfuric acid (H_2SO_4) solution. The electrolytes were prepared shortly before electrolysis experiments. During electrolyzer operation, the catholyte was constantly purged with Ar at 20 sccm. The first gas sample was collected after 20 minutes of continuous operation for complete removal of dissolved CO_2 and even mixing of gaseous products.

For experiments conducted at elevated pressure and temperature, the system was pressurized with inert gas and heated using cell heaters (Dioxide Materials) and heating coils wrapped around catholyte tubes. Heating was controlled by a proportional-integral-derivative (PID) controller and the reported temperature was measured with an in-line thermocouple at the outlet of the membrane electrode assembly. All reported full cell voltages were not iR corrected. The series and charge transfer resistances were analyzed using EIS. Data points were acquired in the frequency range of 10^5 to 0.1 Hz at 75 mA cm^{-2}.

Gas and liquid analysis

Gas chromatography (PerkinElmer Clarus 590) coupled with a thermos conductivity detector (TCD) and flame ionization detector (FID) was used to analyze gas products. Gas samples were analyzed in 1 mL volume and the FE towards gas products were calculated using the following equation:

$$FE_i(\%) = \frac{z_i F P}{RT} \times \nu_i \times \frac{1}{I} \times 100\% \quad (1)$$

where z_i represents moles of electrons needed to produce one mole of the product i, F is the Faraday constant (96485 C mol^{-1}), P represents the pressure at the outlet of the system where the sample is collected (101.325 kPa), R is the ideal gas constant (8.314 J mol^{-1} K^{-1}), T represents the temperature at the outlet of the system where the sample is collected (293 K), ν_i represents the gas flow rate of product i, and I represents the total current. The volumetric gas flow rate was measured at the outlet of the electrolyzer using a bubble column.

The EE toward CO was calculated using the following equation:

$$EE_{CO}(\%) = \frac{1.33\ V}{E_{cell}} \times FE_{CO} \quad (2)$$

where 1.33 V is the thermodynamic cell potential to produce CO and E_{cell} is the measured non-iR corrected full cell voltage.

Proton nuclear magnetic resonance (^{1}H NMR) in water suppression mode was used to analyze electrochemical liquid products. NMR was performed on an Aglient DD2 600 spectrometer in D_2O with trimethylsilylpropanoic acid (TSP) as the internal standard. The FE towards liquid products were calculated using the following equation:

$$FE_i(\%) = m_i \times \frac{z_i F}{It} \times 100\% \quad (3)$$

Where m_i represents moles of product i and t represents the duration of product collection.

Ammonia concentration in the capture solution before degradation experiments and in the DI water trap after degradation experiments were quantified using ultraviolet-visible spectroscopy (UV-vis) by the indophenol blue method[65,66]. The liquid from the DI water trap was used for post-degradation ammonia analysis due to the high volatility of ammonia and interference of amines and amino acids with ammonia detection[67]. Three chemical solutions were prepared: Solution A is a mixture of 1 M NaOH, 5 wt.% salicylic acid, and 5 wt.% sodium citrate, Solution B is 0.05 M NaClO, and Solution C is 1 wt.% sodium

nitroferricyanide. 1 mL of the liquid sample was added to a glass vial. Then, 1 mL of Solution A, 0.5 mL of Solution B, and 0.1 mL of Solution C were added to the vial and shielded from light at room temperature for 2 h. The absorption spectrum was measured using a Lambda 365 UV-vis Spectrometer with spectral range from 190 to 1100 nm. The formation of indophenol blue was determined using the absorbance at a wavelength of 655 nm. The concentration of detected ammonia was calculated using a standard calibration curve.

Anionic O_2 degradation products formate, oxalate, nitrate, and nitrite were quantified using a Thermo Dionex Integrion HPIC system with a CR-ATC 600 trap column, an ADRS 600 suppressor, and a Dionex IonPac AS11 4 × 250 mm anion column. Analysis was performed in isocratic mode with 10 mM KOH as eluent. The amount of amine in the capture solution before and after O_2 degradation experiments were quantified using ^{1}H NMR. Chemical species before and after CO_2 capture were identified using ^{1}H NMR and carbon nuclear magnetic resonance (^{13}C NMR).

Simulated flue gas and direct air capture

To simulate flue gas capture, 80 sccm of a mixed gas stream was purged into the capture solution. The mixed gas stream consisted of 12 sccm CO_2, 57 sccm compressed air, and 11 sccm nitrogen. For DAC, the capture solution was circulated in an Envion Four Seasons humidifier which acted as an air contactor[63]. DI water was added periodically at an average rate of 1.9 mL min^{-1} with a timed pump to compensate for water evaporation and maintain the capture solution reservoir at 2 L. The pH of the capture solution was recorded using a pH probe placed inside the reservoir.

Data availability

All data supporting the findings of this study are available within the paper and the Supplementary Information. Source data are provided with this paper.

References

1. Wen, G. et al. Continuous CO2 electrolysis using a CO2 exsolution-induced flow cell. *Nat. Energy* **7**, 978–988 (2022).
2. Ochedi, F. O., Yu, J., Yu, H., Liu, Y. & Hussain, A. Carbon dioxide capture using liquid absorption methods: a review. *Environ. Chem. Lett.* **19**, 77–109 (2021).
3. Custelcean, R. Direct air capture of CO_2 using solvents. *Annu. Rev. Chem. Biomol. Eng.* **13**, 217–234 (2022).
4. Rochelle, G. T. Amine scrubbing for CO_2 capture. *Science* **325**, 1652–1654 (2009).
5. Alerte, T. et al. Downstream of the CO_2 electrolyzer: assessing the energy intensity of product separation. *ACS Energy Lett.* **6**, 4405–4412 (2021).
6. Li, M., Irtem, E., Iglesias van Montfort, H.-P., Abdinejad, M. & Burdyny, T. Energy comparison of sequential and integrated CO2 capture and electrochemical conversion. *Nat. Commun.* **13**, 5398 (2022).
7. Keith, D. W., Holmes, G., St. Angelo, D. & Heidel, K. A process for capturing CO2 from the atmosphere. *Joule* **2**, 1573–1594 (2018).
8. Xu, Y. et al. Regeneration of direct air CO2 capture liquid via alternating electrocatalysis. *Joule* https://doi.org/10.1016/j.joule.2023.07.011 (2023).
9. Stolaroff, J. K., Keith, D. W. & Lowry, G. V. Carbon dioxide capture from atmospheric air using sodium hydroxide spray. *Environ. Sci. Technol.* **42**, 2728–2735 (2008).
10. Fu, L. et al. Research progress on CO2 capture and utilization technology. *J. CO2 Utilization* **66**, 102260 (2022).
11. Medina-Martos, E. et al. Environmental and economic performance of carbon capture with sodium hydroxide. *J. CO2 Utilization* **60**, 101991 (2022).
12. Li, Y. C. et al. CO_2 electroreduction from carbonate electrolyte. *ACS Energy Lett.* **4**, 1427–1431 (2019).
13. Xiao, Y. C. et al. Direct carbonate electrolysis into pure syngas. *EES Catal.* **1**, 54–61 (2023).
14. O'Brien, C. P. et al. CO_2 electrolyzers. *Chem. Rev.* **124**, 3648–3693 (2024).
15. Rabinowitz, J. A. & Kanan, M. W. The future of low-temperature carbon dioxide electrolysis depends on solving one basic problem. *Nat. Commun.* **11**, 5231 (2020).
16. Ahmad, N. et al. Electrochemical CO2 reduction to CO facilitated by MDEA-based deep eutectic solvent in aqueous solution. *Renew. Energy* **177**, 23–33 (2021).
17. Kim, J. H. et al. The insensitive cation effect on a single atom Ni catalyst allows selective electrochemical conversion of captured CO_2 in universal media. *Energy Environ. Sci.* **15**, 4301–4312 (2022).
18. Langie, K. M. G. et al. Toward economical application of carbon capture and utilization technology with near-zero carbon emission. *Nat. Commun.* **13**, 7482 (2022).
19. Chi, S. & Rochelle, G. T. Oxidative degradation of monoethanolamine. *Ind. Eng. Chem. Res.* **41**, 4178–4186 (2002).
20. Voice, A. K. & Rochelle, G. T. Oxidation of amines at absorber conditions for CO2 capture from flue gas. *Energy Proc.* **4**, 171–178 (2011).
21. Yi, F., Zou, H.-K., Chu, G.-W., Shao, L. & Chen, J.-F. Modeling and experimental studies on absorption of CO2 by Benfield solution in rotating packed bed. *Chem. Eng. J.* **145**, 377–384 (2009).
22. Almajed, H. M. et al. Closing the loop: unexamined performance trade-offs of integrating direct air capture with (bi)carbonate electrolysis. *ACS Energy Lett.* https://doi.org/10.1021/acsenergylett.4c00807 (2024).
23. Feron, P. & Tenasbroek, N. *Greenhouse Gas Control Technologies 7*. vol. II. p. 1153–1158 (Elsevier, 2005).
24. Xu, X. et al. Next generation amino acid technology for CO_2 capture. *J. Mater. Chem. A* **9**, 1692–1704 (2021).
25. Knuutila, H., Aronu, U. E., Kvamsdal, H. M. & Chikukwa, A. Post combustion CO2 capture with an amino acid salt. *Energy Proc.* **4**, 1550–1557 (2011).
26. Jockenhövel, T. & Schneider, R. Towards commercial application of a second-generation post-combustion capture technology — Pilot plant validation of the siemens capture process and implementation of a first demonstration case. *Energy Proc.* **4**, 1451–1458 (2011).
27. Reichl, A. E., Schneider, R., Ohligschläger, A., Rogalinski, T. & Hauke, S. Process development and scale-up for post combustion carbon capture - validation with pilot plant operation. *Energy Proc.* **63**, 6379–6392 (2014).
28. Ramezani, R., Mazinani, S. & Di Felice, R. State-of-the-art of CO_2 capture with amino acid salt solutions. *Rev. Chem. Eng.* **38**, 273–299 (2022).
29. Gusnawan, P., Ganegamage, S., Heagy, M. & Yu, J. Reactive CO2 absorption mechanism of a soybean-based (SBB) solvent containing 18 amino acid salts in polyvinylidene fluoride (PVDF) hollow fiber membrane-based gas-liquid membrane contactor. *Chem. Eng. J.* **399**, 125819 (2020).
30. Brethomé, F. M., Williams, N. J., Seipp, C. A., Kidder, M. K. & Custelcean, R. Direct air capture of CO2 via aqueous-phase absorption and crystalline-phase release using concentrated solar power. *Nat. Energy* **3**, 553–559 (2018).
31. Last, G. V. & Schmick, M. T. *Identification and Selection of Major Carbon Dioxide Stream Compositions*. PNNL–20493, 1019211 http://www.osti.gov/servlets/purl/1019211-QRxIjN/ (2011).
32. Lepaumier, H., Picq, D. & Carrette, P.-L. New amines for CO_2 capture. II. Oxidative degradation mechanisms. *Ind. Eng. Chem. Res.* **48**, 9068–9075 (2009).

33. Sexton, A. J. & Rochelle, G. T. Reaction products from the oxidative degradation of monoethanolamine. *Ind. Eng. Chem. Res.* **50**, 667–673 (2011).
34. Vega, F., Sanna, A., Navarrete, B., Maroto-Valer, M. M. & Cortés, V. J. Degradation of amine-based solvents in CO_2 capture process by chemical absorption: Degradation of amine-based solvents in CO_2 capture process by chemical absorption. *Greenh. Gas. Sci. Technol.* **4**, 707–733 (2014).
35. Vevelstad, S. J., Eide-Haugmo, I., Da Silva, E. F. & Svendsen, H. F. Degradation of MEA; a theoretical study. *Energy Proc.* **4**, 1608–1615 (2011).
36. Nguyen, T., Hilliard, M. & Rochelle, G. Volatility of aqueous amines in CO2 capture. *Energy Proc.* **4**, 1624–1630 (2011).
37. Lee, G. et al. CO2 electroreduction to multicarbon products from carbonate capture liquid. *Joule* **7**, 1277–1288 (2023).
38. Locke, M. J. & McIver, R. T. Effect of solvation on the acid/base properties of glycine. *J. Am. Chem. Soc.* **105**, 4226–4232 (1983).
39. Vijay, S. et al. Unified mechanistic understanding of CO2 reduction to CO on transition metal and single atom catalysts. *Nat. Catal.* **4**, 1024–1031 (2021).
40. Zhang, Z. et al. Porous metal electrodes enable efficient electrolysis of carbon capture solutions. *Energy Environ. Sci.* **15**, 705–713 (2022).
41. Pimlott, D. J. D., Jewlal, A., Mowbray, B. A. W. & Berlinguette, C. P. Impurity-resistant CO_2 reduction using reactive carbon solutions. *ACS Energy Lett.* https://doi.org/10.1021/acsenergylett.3c00133 (2023).
42. Ko, B. H. et al. The impact of nitrogen oxides on electrochemical carbon dioxide reduction. *Nat. Commun.* **11**, 5856 (2020).
43. Jackson, M. N., Jung, O., Lamotte, H. C. & Surendranath, Y. Donor-dependent promotion of interfacial proton-coupled electron transfer in aqueous electrocatalysis. *ACS Catal.* **9**, 3737–3743 (2019).
44. Resasco, J., Lum, Y., Clark, E., Zeledon, J. Z. & Bell, A. T. Effects of anion identity and concentration on electrochemical reduction of CO_2. *ChemElectroChem* **5**, 1064–1072 (2018).
45. Leverick, G. et al. Uncovering the active species in amine-mediated CO_2 reduction to CO on Ag. *ACS Catal.* **13**, 12322–12337 (2023).
46. Safipour, J., Weber, A. Z. & Bell, A. T. Detrimental effects of monoethanolamine and other amine-based capture agents on the electrochemical reduction of CO_2. *ACS Energy Lett.* **8**, 5012–5017 (2023).
47. Siegel, R. E., Pattanayak, S. & Berben, L. A. Reactive capture of CO_2: opportunities and challenges. *ACS Catal.* **13**, 766–784 (2023).
48. Jerng, S. E. & Gallant, B. M. Electrochemical reduction of CO2 in the captured state using aqueous or nonaqueous amines. *iScience* **25**, 104558 (2022).
49. Lee, G. et al. Electrochemical upgrade of CO2 from amine capture solution. *Nat. Energy* **6**, 46–53 (2021).
50. Su, F., Lu, C., Chen, H.-S. & Adsorption Desorption, and thermodynamic studies of CO_2 with high-amine-loaded multiwalled carbon nanotubes. *Langmuir* **27**, 8090–8098 (2011).
51. Pérez-Gallent, E., Vankani, C., Sánchez-Martínez, C., Anastasopol, A. & Goetheer, E. Integrating CO_2 capture with electrochemical conversion using amine-based capture solvents as electrolytes. *Ind. Eng. Chem. Res.* **60**, 4269–4278 (2021).
52. Abas, N. & Khan, N. Carbon conundrum, climate change, CO2 capture and consumptions. *J. CO2 Utilization* **8**, 39–48 (2014).
53. Shen, K. et al. On the origin of carbon sources in the electrochemical upgrade of CO2 from carbon capture solutions. *Joule* **7**, 1260–1276 (2023).
54. Los, P., Rami, A. & Lasia, A. Hydrogen evolution reaction on Ni-Al electrodes. *J. Appl. Electrochem.* **23**, 135–140 (1993).
55. Gabardo, C. M. et al. Continuous carbon dioxide electroreduction to concentrated multi-carbon products using a membrane electrode assembly. *Joule* **3**, 2777–2791 (2019).
56. Burdyny, T. & Smith, W. A. CO_2 reduction on gas-diffusion electrodes and why catalytic performance must be assessed at commercially-relevant conditions. *Energy Environ. Sci.* **12**, 1442–1453 (2019).
57. Kutz, R. B. et al. Sustainion imidazolium-functionalized polymers for carbon dioxide electrolysis. *Energy Technol.* **5**, 929–936 (2017).
58. Kaczur, J. J., Yang, H., Liu, Z., Sajjad, S. D. & Masel, R. I. Carbon dioxide and water electrolysis using new alkaline stable anion membranes. *Front. Chem.* **6**, 263 (2018).
59. Gao, T. et al. Techno-economic analysis and carbon footprint accounting for industrial CO_2 electrolysis systems. *Energy Fuels* **37**, 17997–18008 (2023).
60. Buttler, A. & Spliethoff, H. Current status of water electrolysis for energy storage, grid balancing and sector coupling via power-to-gas and power-to-liquids: a review. *Renew. Sustain. Energy Rev.* **82**, 2440–2454 (2018).
61. Yang, Y. & Li, F. Reactor design for electrochemical CO2 conversion toward large-scale applications. *Curr. Opin. Green Sustain. Chem.* **27**, 100419 (2021).
62. Crandall, B. S. et al. Kilowatt-scale tandem CO2 electrolysis for enhanced acetate and ethylene production. *Nat. Chem. Eng.* **1**, 421–429 (2024).
63. Custelcean, R. et al. Direct air capture of CO_2 with aqueous amino acids and solid bis-iminoguanidines (BIGs). *Ind. Eng. Chem. Res.* **58**, 23338–23346 (2019).
64. Xu, Y. et al. Oxygen-tolerant electroproduction of C_2 products from simulated flue gas. *Energy Environ. Sci.* **13**, 554–561 (2020).
65. Zhao, Y. et al. Ammonia detection methods in photocatalytic and electrocatalytic experiments: how to improve the reliability of NH_3 production rates? *Adv. Sci.* **6**, 1802109 (2019).
66. Lv, C. et al. Selective electrocatalytic synthesis of urea with nitrate and carbon dioxide. *Nat. Sustain.* **4**, 868–876 (2021).
67. Utomo, W. P., Wu, H. & Ng, Y. H. Quantification methodology of ammonia produced from electrocatalytic and photocatalytic nitrogen/nitrate reduction. *Energies* **16**, 27 (2022).

Acknowledgements

The authors gratefully acknowledge support from Shell Global Solutions International B.V., the Natural Sciences and Engineering Research Council of Canada (NSERC) through the Alliance Program, and the Canada Research Chairs Program. Y.C.X. thanks NSERC and Hatch for their support through graduate scholarships. S.S.S. thanks the Government of Ontario for their support through graduate scholarships.

Author contributions

D.S. and E.H.S. supervised the project. Y.C.X. and S.S.S. designed and carried out all experiments. Y.C.X. analyzed the data and wrote the manuscript. Y.Z., Y.C., Z.G., X.W. and J.K. assisted with catalyst preparation. R.K.M. designed the high-pressure system. M.F. performed UV-vis spectroscopy analysis. G.L. and J.E.H. assisted with liquid sample analysis. C.M.G., F.L. and C.O.B. assisted with experiment design. Y.Y. performed XRD analysis. C.Q. and J.Y.H. carried out STEM characterization. P.P. assisted with simulated flue gas experiments. K.H. and P.J.C. provided project direction with an industry perspective and assisted with manuscript editing. All authors discussed the results and assisted during manuscript preparation.

Competing interests

The authors declare no competing interests.

Additional information

Supplementary information The online version contains supplementary material available at https://doi.org/10.1038/s41467-024-51908-3.

Correspondence and requests for materials should be addressed to David Sinton.

Peer review information *Nature Communications* thanks Peng Kang, Xiao Zhang, and the other, anonymous, reviewer(s) for their contribution to the peer review of this work. A peer review file is available.

Reprints and permissions information is available at http://www.nature.com/reprints

Publisher's note Springer Nature remains neutral with regard to jurisdictional claims in published maps and institutional affiliations.

Open Access This article is licensed under a Creative Commons Attribution-NonCommercial-NoDerivatives 4.0 International License, which permits any non-commercial use, sharing, distribution and reproduction in any medium or format, as long as you give appropriate credit to the original author(s) and the source, provide a link to the Creative Commons licence, and indicate if you modified the licensed material. You do not have permission under this licence to share adapted material derived from this article or parts of it. The images or other third party material in this article are included in the article's Creative Commons licence, unless indicated otherwise in a credit line to the material. If material is not included in the article's Creative Commons licence and your intended use is not permitted by statutory regulation or exceeds the permitted use, you will need to obtain permission directly from the copyright holder. To view a copy of this licence, visit http://creativecommons.org/licenses/by-nc-nd/4.0/.

© The Author(s) 2024